Biochimica et Biophysica Acta 1838 (2014) 117–126

Contents lists available at ScienceDirect

Biochimica et Biophysica Acta

journal homepage: www.elsevier.com/locate/bbamem

Structure and orientation study of Ebola fusion peptide inserted in lipid membrane models

Audrey Agopian, Sabine Castano *

CBMN-UMR 5248 CNRS, Université de Bordeaux, IPB, Allée Geoffroy Saint Hilaire, 33600 Pessac, France

ARTICLE INFO

Article history:
Received 17 May 2013
Received in revised form 4 September 2013
Accepted 9 September 2013
Available online 18 September 2013

Keywords:
Ebola fusion peptide
Lipid/peptide interaction
Secondary structure
Viral fusion mechanism
IR spectroscopy
Ellipsometry

ABSTRACT

The fusion peptide of Ebola virus comprises a highly hydrophobic sequence located downstream from the N-terminus of the glycoprotein GP2 responsible for virus–host membrane fusion. The internal fusion peptide of GP2 inserts into membranes of infected cell to mediate the viral and the host cell membrane fusion. Since the sequence length of Ebola fusion peptide is still not clear, we study in the present work the behavior of two fusion peptides of different lengths which were named EBO17 and EBO24 referring to their amino acid length. The secondary structure and orientation of both peptides in lipid model systems made of DMPC:DMPG:cholesterol:DMPE (6:2:5:3) were investigated using PMIRRAS and polarized ATR spectroscopy coupled with Brewster angle microscopy. The infrared results showed a structural flexibility of both fusion peptides which are able to transit reversibly from an α-helix to antiparallel β-sheets. Ellipsometry results corroborate together with isotherm measurements that EBO peptides interacting with lipid monolayer highly affected the lipid organization. When interacting with a single lipid bilayer, at low peptide content, EBO peptides insert as mostly α-helices mainly perpendicular into the lipid membrane thus tend to organize the lipid acyl chains. Inserted in multilamellar vesicles at higher peptide content, EBO peptides are mostly in β-sheet structures and induce a disorganization of the lipid chain order. In this paper, we show that the secondary structure of the Ebola fusion peptide is reversibly flexible between α-helical and β-sheet conformations, this feature being dependent on its concentration in lipids, eventually inducing membrane fusion.

1. Introduction

The Ebola virus is one of the most virulent pathogens for humans and primates. It has caused several outbreaks in central Africa in the past decade and currently no treatments or vaccines are approved yet. Ebola virus is an enveloped virus that belongs to the *filoviridae* family. It causes severe hemorrhagic fever that is often lethal in humans. Early target cells are monocytes, macrophages, dendritic cells and hepatocytes then the infection rapidly spreads to the viral organs of the host. Infection of a target cell by enveloped virus requires fusion between the viral enveloped and host cell membrane. The membrane fusion process is a common feature of enveloped viruses and is mediated by a glycoprotein (GP) that acts as a membrane fusion protein. The Ebola GP is a class I fusion protein that forms trimeric spikes on the virion surface [1]. During the maturation of the virion, GP is activated by proteolytic cleavage into two parts: GP1 and GP2, connected by a disulfide bond. In all the class I fusion protein, the first subunit binds to the cell receptors while the second subunit mediates the fusion between viral and host cell membranes. For Ebola, the fusion process is mediated by the virally encoded glycoprotein GP2 that contains a highly hydrophobic sequence generally referred as the fusion peptide which initiates the fusion event by anchoring glycoprotein GP2 to the cell membrane surface. Unlike other class I fusion proteins, the Ebola fusion peptide is located within the GP2 structure downstream from the N-terminus. This conserved peptide sequence is absolutely required for the fusogenic activity of the glycoprotein GP2 but its structural and functional determinants remain unknown. Previous studies showed that endosome allows pH activating cathepsin L and B activities that is required for viral fusion to occur where GP2 undergoes a subsequent conformational change exposing the fusion peptide to the host membrane [2–4]. However, how Ebola fusion peptide binds to the membranes and induces fusion remains poorly understood.

Several studies about Ebola fusion peptide have been done in different conditions and different mimetic membrane environments, partly leading to inconsistent results. In general, Ebola fusion peptide can adopt different structures depending on its environment. Moreover, the exact peptide sequence involved in the fusion, which was initially predicted by Gallaher et al. [5] is not well defined to date, as numerous studies used different fusion peptide lengths. Freitas et al. [6] utilized Ebola fusion peptide composed of 16 amino acids, EBO16 (524–539

Abbreviations: DMPC, dimyristoyl-phosphatidylcholine; DMPG, dimyristoyl-phosphatidylglycerol; DMPE, dimyristoyl-phosphatidylethanolamine; PMIRRAS, polarization modulation infra-red reflection absorption spectroscopy; ATR, attenuated total reflection spectroscopy; BAM, Brewster angle microscopy; Ri, lipid to peptide ratio

* Corresponding author at: CBMN/University Bordeaux 1, Allée Geoffroy Saint Hilaire, F-33600 Pessac, France. Tel.: +33 5 40 00 68 48; fax: +33 5 40 00 22 00.
E-mail address: s.castano@cbmn.u-bordeaux.fr (S. Castano).

0005-2736/$ – see front matter © 2013 Elsevier B.V. All rights reserved.
http://dx.doi.org/10.1016/j.bbamem.2013.09.003

from GP2) and determined its secondary structure by circular dichroïsm (CD) and nuclear magnetic resonance (NMR). They showed a random coil–helix transition when they added SDS micelles to an insoluble water-diluted EBO16 solution. The NMR structure of EBO16 showed that in the presence of mimetic membranes, the peptide adopts a central 3_{10}-helix structure stabilized by aromatic interaction between amino acids Trp8 and Phe12. Suárez et al. [7] used a 17 amino acid sequence as fusion peptide (EBO_{GE}: 524–540 from GP2) and also showed by UV CD spectroscopy structural transition between random-coil in aqueous buffer and an α-helix structure induced by increasing concentration of TFE. Moreover, they demonstrated by IR spectroscopy that in association to PC/PI (1:2) vesicles, the fusion peptide undergoes a conformational change from an α-helix to an anti-parallel β-structure, presumably induced by the presence of calcium. In fact, the α-helical structure seems to be related to the ability of the peptide to induce destabilization of the membrane while the presence of Ca^{2+} provocated a conformational transition of the peptide to a β-sheet structure [7–9]. In a more recent study [10], Freitas et al. suggested that although their EBO16 fusion peptide adopts a β-sheet structure, it was only able to induce PC:PE:SPM:Chol liposome aggregation but not fusion. They also showed by experiments of raft aggregation and cell–cell fusion that EBO16 fusion peptide is able to use lipid raft domains enriched in cholesterol [11] as a target for virus entry into cells. This suggests an important role of cholesterol since cholesterol depleted cells have impaired EBO virus glycoprotein-pseudotype-virion entry and fusion [12]. They also demonstrated that the fusion peptide EBO16 can induce lipid mixing of the living Vero cells even in absence of Ca^{2+}. In the same study, EBO16 was proposed to lie parallel to the membrane anchored by the aromatic amino acids, Trp8 and Phe12. In another study conducted by Adam et al. [13], they used a shorter peptide of 11 amino acid long (524 to 534) capable of liposome destabilization and fusion. They also analyzed its behavior in a hydrophobic/hydrophilic environment by molecular modeling. They proposed a mechanism where the peptide is obliquely inserted in the host membrane and further able to destabilize it.

The aim of the present work was to clarify the inconsistencies between the previously published data and to improve our understanding of the fusion mechanism by which the Ebola fusion peptide inserts into lipid membrane. The structural behavior of the individual Ebola fusion peptide as well as that bound to a lipid membrane model has thus been investigated using several infrared (IR) spectroscopy techniques: PMIRRAS at the air/water interface of the peptides alone and inserted into lipid monolayers and ATR spectroscopy of peptides inserted in bi- and multi-bilayers. Investigations at the air/water interface were combined with ellipsometric measurements to analyze the morphology of the layers. The peptide orientation given by IR experimental results were analyzed using spectral simulation. Two peptide sequences were studied: the 17 (residues 524–540, EBO17) and the 24 (residues 524–547, EBO24) amino acid consensus sequences.

2. Materials and methods

2.1. Lipids and peptides

Lipids (DMPC, DMPG, cholesterol and DMPE) were purchased from Sigma. The Ebola fusion peptides EBO17: GAAIGLAWIPYFGPAAE and EBO24: GAAIGLAWIPYFGPAAEGIYTEGL were purchased from GenScript (Piscataway, USA). EBO17 and EBO24 were solubilized in hexafluoroisopropanol (HFIP) from Sigma at micromolar concentrations. Peptide concentrations were calculated from the absorbance at 280 nm using a molar extinction coefficient ε_{280} of 7000 $M^{-1}\cdot cm^{-1}$ for EBO17 and ε_{280} of 8400 $M^{-1}\cdot cm^{-1}$ for EBO24. The molar extinction coefficient of the peptides has been determined using the formula $\varepsilon_{280nm} = 5600 \times n_W + 1400 \times n_Y$ which takes into account the individual extinction coefficient of the amino acids W and Y.

2.2. Film formation and surface pressure measurements

Monolayer experiments were performed on a computer-controlled Langmuir film balance (Nima Technology, Coventry, England). The rectangular trough and the barrier were made of Teflon. The surface pressure (π) was measured by the Wilhelmy method using a filter paper plate. The trough was filled with a saline solution (150 mM NaCl, pH 5.6) using ultra pure water (MilliQ, Millipore). The experiments were carried out at 22 ± 2 °C. Pure peptide films were obtained by spreading of few μl of HFIP peptide stock solutions at the air/water interface. The mixed lipids/peptides at the defined lipid to peptide ratio, Ri was obtained by co-spreading of the lipid/peptide mixture at the water surface. The monolayer lipid composition used was DMPC:DMPG:cholesterol:DMPE (6:2:5:3). After ~15 min of stabilization, the film was slowly compressed up to 40 $mN\cdot m^{-1}$ and decompressed at the same rate speed than during the compression (8 $Å^2\cdot molecule^{-1}\cdot min^{-1}$).

2.3. PMIRRAS spectroscopy

PMIRRAS spectra were recorded on a Nicolet Nexus 870 spectrometer equipped with a photovoltaic HgCdTe detector cooled at 77 K. Spectra were obtained by performing 800 scans at a resolution of 8 cm^{-1}. Briefly, PMIRRAS combines FT-IR reflection spectroscopy with fast polarization modulation of the incident beam between parallel (p) and perpendicular (s) polarizations. The differential reflectivity spectrum is obtained using a two-channel processing signal. To remove the contribution of liquid water absorption and the dependence on Bessel functions, the monolayer spectra are divided by that of the subphase. With an incidence angle of 75°, transition moments preferentially oriented in the plane of the interface give intense and upward oriented bands, while perpendicular ones give weaker and downward oriented bands [14].

2.4. ATR spectroscopy of the fusion peptide inserted in a lipid bilayer

Small unilamellar vesicles (SUV) composed of DMPC:DMPG: cholesterol:DMPE (6:2:5:3) were prepared pure or mixed with the fusion peptide at a defined molar ratio, Ri. For pure lipid SUV, lipids were first dissolved in chloroform and mixed at the desired ratio. The solvent was then evaporated giving a lipid film. SUV were then prepared by tip sonication after direct hydration of the lipid film with a solution of D_2O containing 150 mM NaCl. For the preparation of the SUV containing the mixed fusion peptide/lipids, the fusion peptide powder is first dissolved in HFIP then mixed with the lipids in chloroform at the desired ratio. Solvents were evaporated before hydration by D_2O and tip sonication for SUV formation. SUV were then burst on a germanium ATR crystal to form a single bilayer which is controlled by the measurement of the absolute IR intensity.

ATR spectra were recorded on a Nicolet 6700 spectrometer Thermo Scientific equipped with a MCT detector cooled at 77 K. Since ATR spectroscopy is sensitive to the orientation of the structures [15–17], spectra were recorded with parallel (p) and perpendicular (s) polarizations of the incident light with respect to the ATR plate. 400 scans were recorded at a resolution of 8 cm^{-1}. All the orientation information is then contained in the dichroïc ratio $R_{ATR} = Ap/As$, where Ai respectively represents the absorbance of the considered band at p or s polarization of the incident light.

2.5. Ellipsometric measurements

The morphology of pure peptides or mixed lipids with the peptides was observed at the air/water interface using an ellipsometer iElli2000 microscope (NFT, Göttinger, Germany) mounted on a Langmuir trough. The microscope was equipped with a doubled frequency Nd:Yag laser (532 nm, 50 mW), a polarizer, a compensator, an analyzer and a CCD camera. The spatial resolution of the pictures with the 10× magnification lens was about 2 μm and the image size was 600 × 450 μm. For

ellipsometric measurements, the imaging ellipsometer works at an incidence angle close to the Brewster angle (54.6°). It operates using the principle of a classical null ellipsometer [18]. The ellipsometric angles (Δ, Ψ) are determined from polarizer and analyzer azimuths at extinction; Δ and Ψ are related to the optical properties of the sample.

In ultra-thin film conditions, Δ is proportional to the film thickness. The comparison of the experimental data with a computerized optical modeling included in the ellipsometer software allowed to provide an estimation of the film thickness when a value of refractive index can be obtained. Since it is difficult to determine an experimental refractive index value, we choose 1.50 for the EBO peptides as it was used in a previous work concerning the fusion peptide FP23 of HIV [19]. Indeed, in the literature, variations between 1.45 [20] and 1.53 [21,22] can be encountered for protein and peptide depending on the amount of water taken into account. Concerning lipids, anisotropic refractive indices between 1.44 [23] and 1.50 [24] were reported for DMPC in the literature. Therefore, we use an intermediate value of 1.46 to perform thickness estimations [19].

3. Results

3.1. Morphological and structural study of the fusion peptides EBO17 and EBO24 at the air/water interface

3.1.1. EBO17 at the air/water interface

The Brewster angle microscope (BAM) images of the pure EBO17 layer at increasing surface pressures from 5 to 20 mN/m (Fig. 1) display a progressive increase of the averaged normalized gray level until 20 mN/m. Every picture shows a very stable homogeneous surface of the peptide layer even at low pressures such as 2 mN/m (data not shown) and the peptide film appears brighter during compression. The thickness of the layer was estimated by ellipsometry using a constant refractive index of 1.50 for the peptide (cf. Materials and methods section). As the peptide film is compressed, estimated thickness increases from 9 Å (Δ = 354.37°, Ψ = 2.42) at 5 mN/m to 14 Å (Δ = 352.20°, Ψ = 2.42°) at 20 mN/m.

The PMIRRAS spectra at the air/water interface of the EBO17 peptide film during compression from 1 to 20 mN/m displayed well resolved but broad amide I bands between 1600 and 1700 cm^{-1} and amide II bands centered around 1530 cm^{-1} (Fig. 2A). At lower surface pressures (below 7 mN/m), the amide I band is mainly centered around 1652 cm^{-1} reflecting a main content of α-helix. A shoulder around 1630 cm^{-1} also shows a β-sheet contribution and secondary derivative (not shown) displays also contributions around 1642 cm^{-1} and 1670 cm^{-1} respectively a characteristic of random and β-turn structures [16,25,26]. During compression of the peptide film (up to 15 mN/m), there is a shift of the position of the main amide I band. The contribution of the α-helix (around 1652 cm^{-1}) decreases in favor of two other main contributions centered around 1630 cm^{-1} and 1690 cm^{-1} a characteristic of antiparallel β-sheets which become predominant at 20 mN/m. Since these two contributions display positive bands, one can assume that antiparallel β-sheets are mainly oriented flat on the air/water interface plane [27,28].

During decompression down to 10 mN/m, the main component remains centered around 1630 cm^{-1} with a shoulder at 1690 cm^{-1} revealing the predominance of β-sheet structures. PMIRRAS spectra at these intermediate surface pressures also contain shoulder at 1655 cm^{-1} reflecting a small content of α-helix. At lower surface pressure (below 7 mN/m), the main band is centered around 1655 cm^{-1}, mainly a characteristic of α-helical structures.

This experiment suggests that EBO17 undergoes a conformational transition from an α-helix to an antiparallel β-sheet when surface pressure is increased and that this transition is reversible when surface pressure is decreased. This result is confirmed during a second compression/decompression cycle where the fusion peptide EBO17 reversibly undergoes a transition from α-helix to β-sheet.

3.1.2. EBO24 at the air/water interface

Like EBO17, EBO24 at the air/water interface shows homogeneous and stable films as depicted in Fig. 1. The gray level intensity increases as the surface pressure rises and the thickness can be estimated by ellipsometry. EBO24 forms film with an estimated thickness of about 10 Å (Δ = 354.29°, Ψ = 2.41°) at 5 mN/m up to 17 Å (Δ = 350.99°, Ψ = 2.41°) at 20 mN/m.

PMIRRAS spectra of EBO24 at the air/water interface (Fig. 2B) display a main amide I band around 1653 cm^{-1} at surface pressures below 15 mN/m showing that EBO24 is mainly structured as an α-helix. An equivalent of "full width at half maximum" (FWHM) on the main amide I band can be estimated: FWHM = 74 cm^{-1} at 15 mN/m and 51 cm^{-1} at 20 mN/m for EBO17 compared to 51 cm^{-1} and 45 cm^{-1} for EBO24 at the same surface pressures. This comparison clearly shows that the amide I band of EBO24 is thinner compared to the one of EBO17 showing better folding of EBO24. Then one can assume that the amide contributions are mainly due to the α-helical structure.

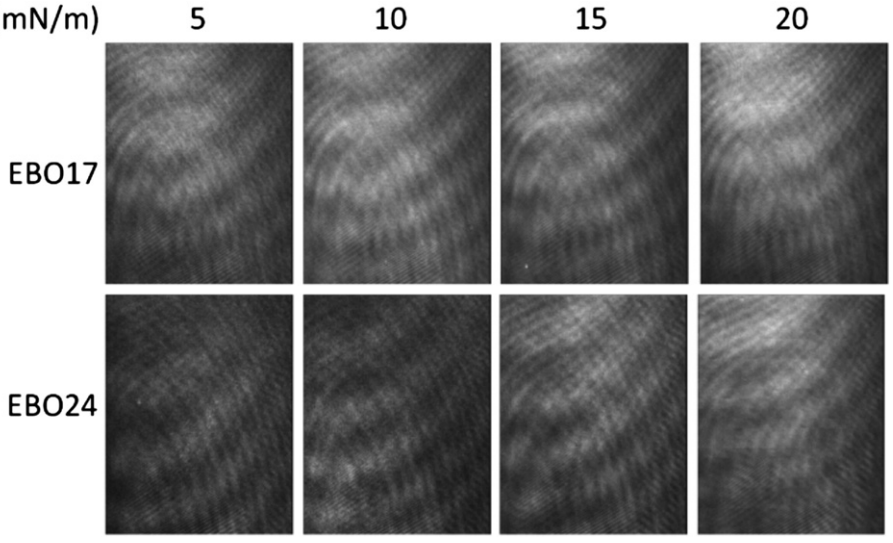

Fig. 1. BAM images of EBO17 alone at the air/water interface. For EBO17: at 5 mN/m, GL = 42, at 10 mN/m, GL = 48, at 15 mN/m, GL = 52, at 20 mN/m, GL = 53. For EBO24: at 5 mN/m, GL = 35, at 10 mN/m, GL = 39, at 15 mN/m, GL = 45, at 20 mN/m, GL = 54. Exposition time for each image was fixed at 1/50 s. Sub-phase: saline solution, 150 mN NaCl, pH 5.6. GL: gray level.

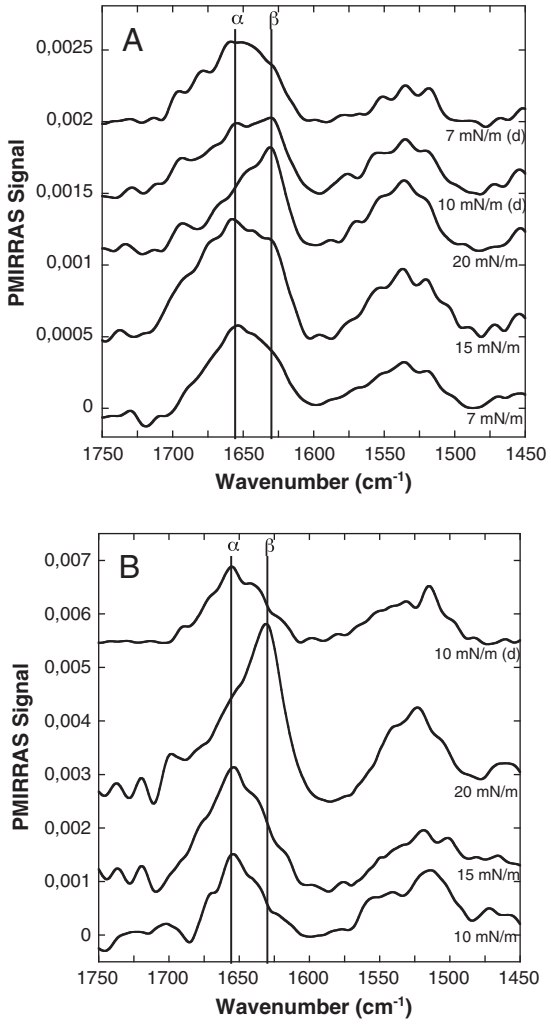

Fig. 2. PMIRRAS spectra of the fusion peptides alone at the air/water interface during compression and decompression: EBO17 (A) EBO24 (B).

Amide I to Amide II ratio is higher than 2 which is a characteristic of a helix axis lying parallel to the interface plane [27,28]. During compression of the peptide monolayer up to 20 mN/m, there is a shift of the maximum of the main amide I band to 1630 cm^{-1} with a second contribution at 1690 cm^{-1} characteristic of antiparallel β-sheet structure of EBO24. Again, the positive contributions of these two β-sheet bands allow to propose a flat orientation of the β-sheet structure of the peptide with respect to the interface plane. During decompression down to 10 mN/m, the amide I band shifts back to a main contribution at approximately 1653 cm^{-1} which is a characteristic of a major α-helical structure. Then as observed for EBO17, EBO24 undergoes a reversible structural transition from an α-helix to an antiparallel β-sheet which can be controlled by changing surface pressure.

3.2. Morphological and structural study of EBO17 and EBO24 inserted into a lipid monolayer

3.2.1. Study of the morphology and the stability of mixed EBO17 or EBO24 with lipid monolayers

To investigate the changes in morphology and stability induced by EBO peptides in interaction with the DMPC:DMPG:cholesterol:DMPE monolayer at the molar ratio 6:2:5:3, we first studied the morphology and the stability of the lipid alone in the surface pressure range from 5 to 30 mN/m. The molecular area of approximately 45 $Å^2$/mol before collapse obtained from the surface pressure (∏)–area (A) isotherm of the lipid monolayer (Fig. 3) is consistent with that of Langmuir monolayers mainly composed of phospholipids with dimyristoylacyl chains [29]. The isotherm is reversible during decompression showing a very small hysteresis which suggests that there is no loss of material into the subphase. BAM pictures (Fig. 4, first row micrographs) show that the surface is homogeneous whatever the surface pressure during compression and decompression. Such an observation could be surprising since the monolayer contains DMPE and cholesterol which display high phase transition temperatures (>49 °C) compared to DMPC and DMPG (23 °C), then one can expect to observe segregation of lipids in the monolayer. Taking into account the large content in cholesterol of the monolayer, the observation of such a homogeneous film can probably be explained by attractive interactions between the different phospholipids and cholesterol as previously reported [30]. Ellipsometric measurements and thickness estimations using a refractive index of 1.46 for the lipids (cf. Materials and methods section) lead to 13 ± 1 Å (Δ = 351.01°, Ψ = 2.39°) for the thickness of the lipid monolayer at 5 mN/m, 14 ± 1 Å (Δ = 350.45°, Ψ = 2.39°) at 15 mN/m and 15 ± 1 Å (Δ = 349.98°, Ψ = 2.39°) at 30 mN/m.

BAM pictures and compression isotherms of EBO peptides inserted into a lipid monolayer are recorded after co-deposition at the air/water interface of a peptide/lipid (DMPC:DMPG:cholesterol:DMPE 6:2:5:3) mixture at a defined lipid to peptide ratio, Ri = 20 or Ri = 50. When EBO peptides are inserted into the lipid monolayer, important changes in the morphology of the layer are observed compared to the lipid alone (Fig. 4). At low surface pressure (5 mN/m), whatever the peptide and the lipid/peptide ratio Ri (20 or 50) very heterogeneous surfaces are observed which are characterized by fluid circular domains in a less dense phase (dark background). If at Ri = 50, there is no important thickness difference between the two phases (14–15 Å for the denser compared to 12–13 Å), it is noteworthy that at high peptide content (Ri = 20), the main thickness of the surrounding phase is very low (<7 Å) as if the peptides lead to a condensation of the material in the layer. When the surface pressure increases to 15 mN/m, whatever the peptide and the Ri, there is a homogenization of the surface which appears to be more rigid compared to the lipid alone with a mean thickness around 13 ± 1 Å. At high surface pressure (30 mN/m), whatever the peptide and the Ri, pictures are characterized by a bright network formed by long and thin interconnected filaments of high thickness (>18 Å) in a homogeneous phase of 14 ± 1 Å thick. The decompression down to 15 mN/m leads back to a homogenization of the surface which appears highly comparable to the lipid alone both in the thickness (14 ± 1 Å thick) and fluidity. At low surface pressures (5 mN/m),

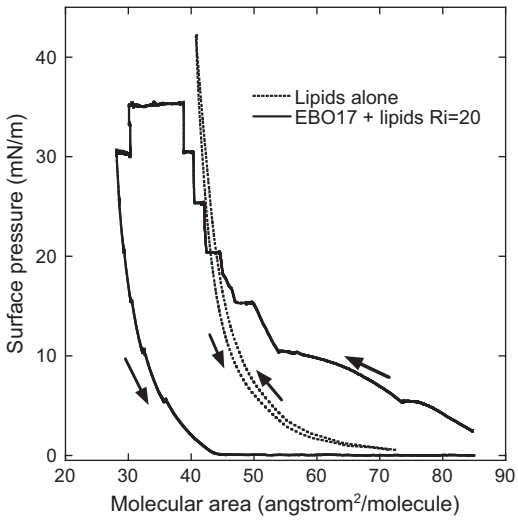

Fig. 3. Surface pressure (∏)–molecular area ($Å^2$/molecule) isotherms of a lipid monolayer composed of DMPC:DMPG:cholesterol:DMPE (6:2:5:3) in the absence (dash line) and in the presence of EBO17 at Ri = 20 (solid line). Plateaus correspond to compression stops.

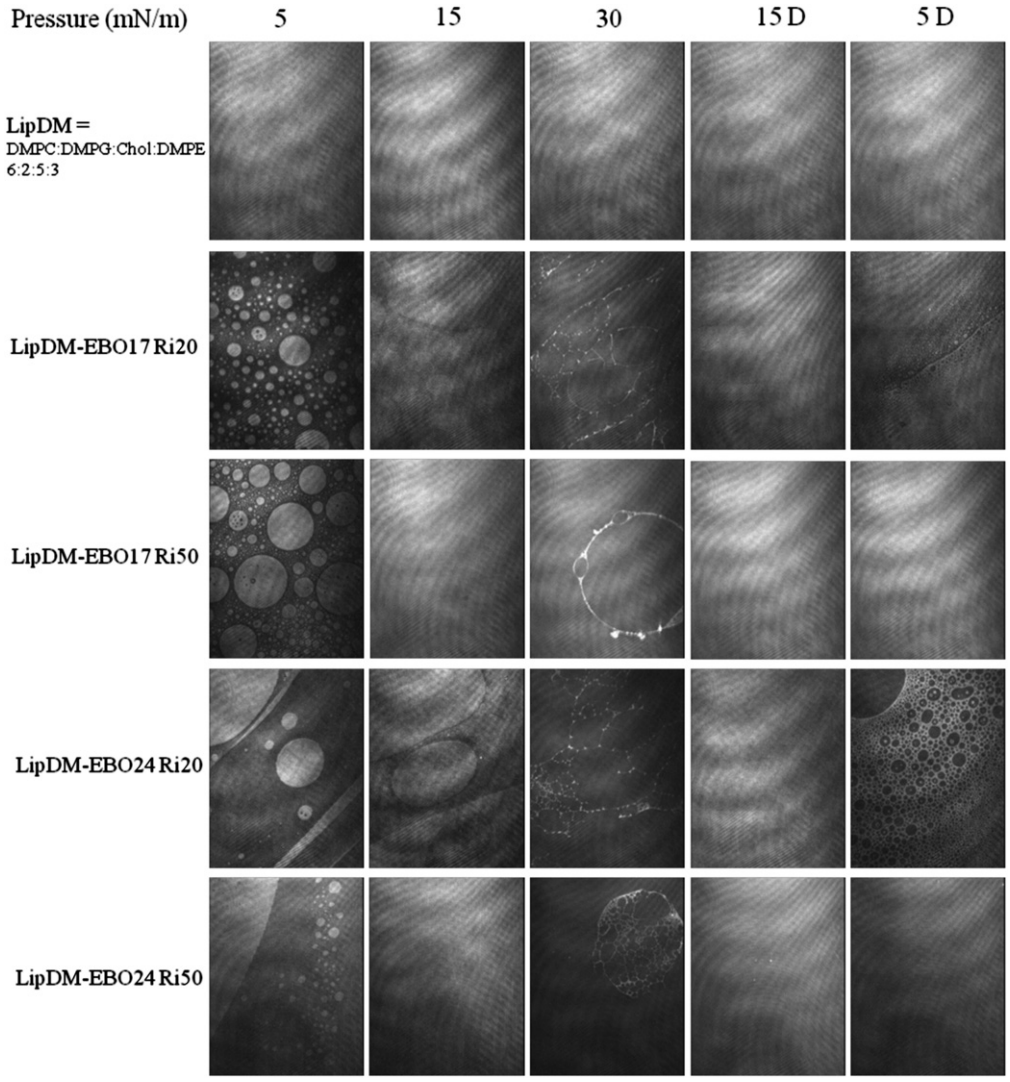

Fig. 4. BAM images of a lipid monolayer composed of DMPC:DMPG:cholesterol:DMPE 6:2:5:3 (first line), mixed DMPC:DMPG:cholesterol:DMPE (6:2:5:3)/EBO17 at Ri = 20 (second line) and Ri = 50 (third line) and mixed DMPC:DMPG:cholesterol:DMPE (6:2:5:3)/EBO24 at Ri = 20 (fourth line) and Ri = 50 (last line). Exposition time for each image was fixed at 1/50 s. Subphase: saline solution, 150 mN NaCl, pH 5.6.

whatever the peptide, the monolayer is homogeneous at Ri = 50 while some heterogeneities remain at Ri = 20 but in both cases, the mean thickness is close to the one of the lipid monolayer alone (13 ± 1 Å). Despite these differences, whatever the peptide and the Ri, the changes observed in morphology during compression are not reversible during decompression.

An explanation is given by the compression isotherm (Fig. 3) of the mixed EBO17/lipid monolayer at Ri = 20. Indeed, at the beginning of the compression (low surface pressures), the molecular area is larger for the mixed EBO17/lipid monolayer compared to that of the lipid alone because of the contribution of the peptide. When the molecular area decreases, the shape of the isotherm is different from that of the lipid alone (weaker slope) showing the influence of the peptide. At high surface pressures (up to 20 mN/m), the isotherm of the mixed EBO17/lipid monolayer intersects the one of the lipid alone. We observe changes of slope in the isotherm which correspond to stop of compression at a defined pressure. The observed plateaus demonstrate that it becomes difficult to maintain compression levels, showing an instability of the mixed EBO17/lipid monolayer and the loss of material in the subphase. The decompression shows an important hysteresis and the shape of the isotherm is close to the one of the lipid alone. The same behavior has been observed whatever the peptide (EBO17 and EBO24) and whatever the Ri (20 or 50) (data not shown). These results show that whatever the EBO peptide and the Ri tested, the presence of the peptide destabilizes the lipid monolayer.

3.2.2. PMIRRAS structure study of mixed EBO17 or EBO 24/lipid monolayers

PMIRRAS spectra of EBO peptides inserted into a DMPC:DMPG: cholesterol:DMPE (6:2:5:3) lipid monolayer are recorded as previously described. The mixed monolayer was compressed from 5 to 40 mN/m then decompressed down to 5 mN/m. PMIRRAS spectra were recorded at different surface pressures (Fig. 5). Every spectrum shows a band centered around 1737 cm^{-1} characteristics of the (C═O) ester stretching vibration. The δ (CH_2) bending vibration of acyl chains at 1467 cm^{-1} can also be observed on the majority of the spectra except for the 5 mN/m spectrum during compression of EBO17 (Ri = 50) as well as those at 5 and 15 mN/m (compression) of EBO24 (Ri = 20) where the band is difficult to distinguish from the noise [31]. Whatever EBO17 or EBO24 and the lipid ratio Ri = 50 or Ri = 20, the same behavior during compression and decompression occurs. At the beginning of the compression (5 mN/m), a large intensity of the amide I band of the peptide can be observed, which is consistent with the substantial Ri. This band is centered at approximately 1653 cm^{-1}, which is a characteristic of a major α-helix folding. The lack or very weak contribution of the amide II band shows that the helix is mainly oriented with its axis parallel to the monolayer. At Ri = 50 mainly on EBO17 spectrum, a

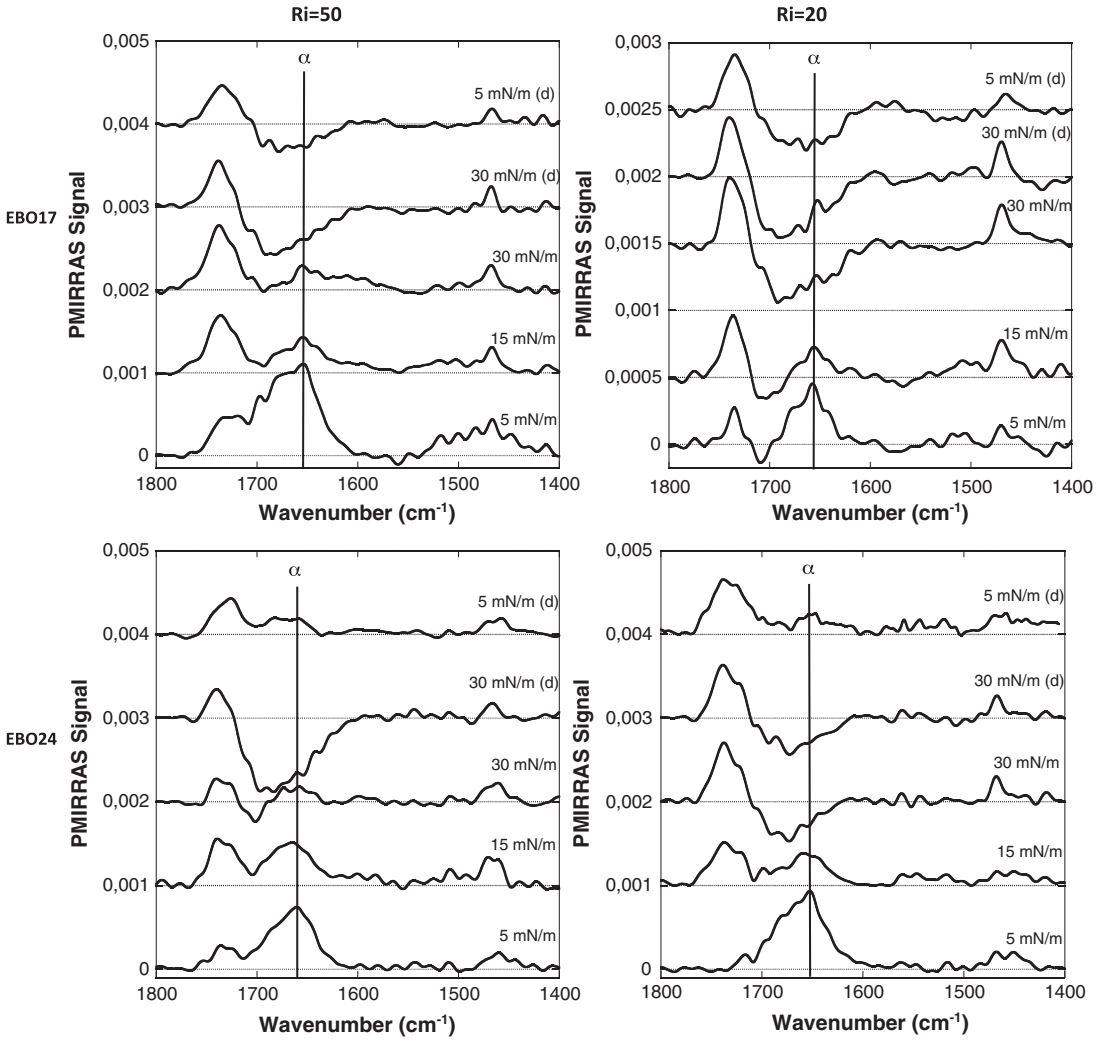

Fig. 5. PMIRRAS spectra of EBO17 and EBO24 inserted in a lipid monolayer of DMPC:DMPG:cholesterol:DMPE (6:2:5:3) during compression and decompression (d). Top: EB017, bottom: EBO24, left: Ri = 50, right: Ri = 20. Subphase: saline solution, 150 mN NaCl, pH 5.6.

shoulder around 1673 cm^{-1} also shows contributions of β-turn structures as it was observed for the peptide alone. As the surface pressure increases (up to 30 mN/m), the absorption bands of the lipids increases due to the concentration of the molecules under the beam whereas the amide I band of the peptides decreases progressively and sometimes disappears. To be sure that this phenomenon was not due to an optical effect, the ratio of the lipid/peptide spectrum towards the spectrum of a pure lipid monolayer at the same surface pressure was performed and no amide I band was observed (data not shown). This again demonstrates the instability of the mixed EBO/lipid monolayer at high surface pressures and the exclusion of EBO peptide (or EBO peptide/lipid complexes) from the monolayer. During decompression from 40 mN/m down to 5 mN/m, the amide I band does not appear again (EBO17), or weakly (EBO24) and the main structure remains α-helical.

3.3. Study of EBO17 and EBO24 peptides inserted into lipid bilayers by ATR

We further investigated the behavior of the peptides inserted into lipid bilayers (either in a single supported lipid bilayer or in MLV in solution) made of the same lipid mixture DMPC:DMPG:cholesterol:DMPE (6:2:5:3), these model being closer to natural membranes. We hence performed polarized ATR experiments in order to analyze the structure (and the orientation when it is possible) of the fusion peptides in such membrane models as well as perturbations induced by the peptide on the organization of the lipids.

3.3.1. EBO17 and EBO24 inserted into a single supported lipid bilayer at Ri = 150 by ATR spectroscopy

The pure lipid or mixed EBO/lipid bilayers adsorbed on a germanium ATR crystal were obtained by spontaneous fusion of small unilamellar vesicles (SUV) of pure lipid or mixed EBO/lipid at the defined Ri. Fig. 6A and B displays the ATR spectra obtained in the 1800–1500 cm^{-1} region. The band around 1735 cm^{-1} corresponds to the (C═O) ester of the lipids while the 1700–1600 cm^{-1} domain corresponds to the amide I. The amide I region was analyzed and the secondary structure content was evaluated from the analysis of the amide I band shape and curve fitting [15]. The 1684 ± 1 cm^{-1}, 1633 ± 1 cm^{-1} and 1623 ± 1 cm^{-1} bands were assigned to β-sheets, the 1661 cm^{-1} and 1652 ± 1 cm^{-1} bands to α-helices, the 1642 ± 2 cm^{-1} band to random structures and the 1671 ± 2 cm^{-1} band to β-turns. The results are presented in Table 1. It can be seen that with the burst SUV at Ri = 150, EBO17 and EBO24 display a quite comparable structural composition with a predominant α-helical structure (37.7% and 43.0% respectively). Using the p- and s-polarized spectra, we then estimated the dichroïc ratio of the amide I band of the α-helix, we obtain R_{ATR} (amide I/α-helix) > 2.4 which allows to estimate that the α-helix is mainly perpendicular to the plane of the bilayer [19].

To investigate the consequence of the EBO peptide insertion on the organization of the lipid acyl chains in the bilayer, the shift of the bands corresponding to antisymmetric and symmetric stretching modes of the methylene groups, $\nu_s(CH_2)$ and $\nu_{as}(CH_2)$, respectively,

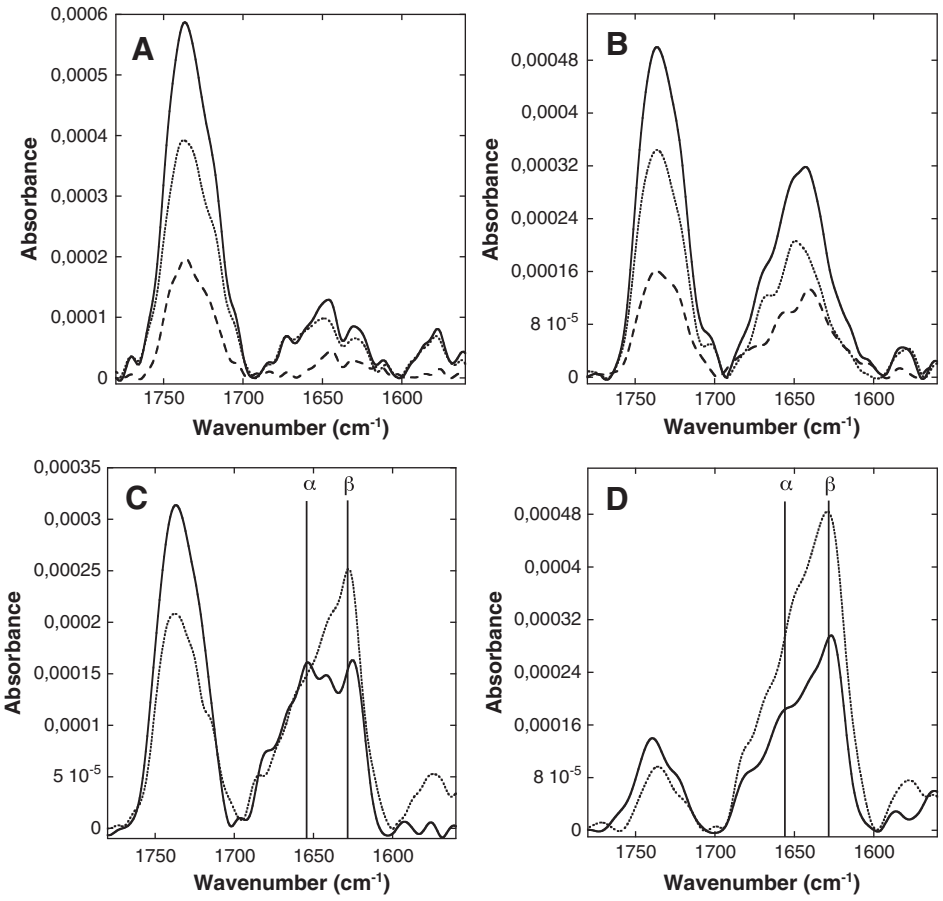

Fig. 6. ATR spectra in the amide I region of EBO17 and EBO24 inserted into lipid bilayer DMPC:DMPG:cholesterol:DMPE (6:2:5:3) hydrated by D_2O + 150 mM NaCl. A: EBO17 at Ri = 150 in a supported lipid bilayer: isotropic spectrum (solid line), p-polarized spectrum (dotted line), s-polarized spectrum (dashed line), B: EBO24 at Ri = 150 in a supported lipid bilayer: isotropic spectrum (solid line), p-polarized spectrum (dotted line), s-polarized spectrum (dashed line), C: EBO17 (solid line) and EBO24 (dotted line) in MLV Ri = 100, D: EBO17 (solid line) and EBO24 (dotted line) in MLV Ri = 20.

was measured (Table 2). Indeed, the wavenumbers of these bands are known to be sensitive to changes in the configuration of the acyl chains, in chain mobility and packing [32–35]. The $\nu_s(CH_2)$ and $\nu_{as}(CH_2)$ of 2851.7 and 2920.7 cm^{-1} respectively for the bilayer alone are characteristic of quite well ordered acyl chains, which is consistent with a bilayer composed of phospholipids with phase transition temperature higher than 23 °C. When EBO peptides interact with the bilayer, there is an average decrease of 1.6 ± 0.3 cm^{-1} in the wavenumbers of the $\nu_s(CH_2)$ and $\nu_{as}(CH_2)$ which shows an increase of the chains order due to the EBO peptide insertion (Fig. 7, Table 2). This is confirmed by the evolution of the dichroïc ratio (R_{ATR}) of the $\nu_s(CH_2)$ band of lipid chains which was measured on the polarized ATR spectra (Table 2). Indeed, since the transition moment for the $\nu_s(CH_2)$ lies perpendicular to the chain axis, the introduction of order or disorder alters the direction of the main chain with respect to the normal of the ATR crystal. The dichroïc ratio is then expected to provide a sensitive and quantitative indicator of acyl chain order by estimating the average C–C–C angle of the lipid carbon chains with the normal to the interface [19]. Here, the R_{ATR} decreases when EBO peptides interact with the lipids, compared to the lipid alone (Table 2). This corresponds to a reorientation of the

Table 1
Wavenumbers and secondary structure contents for EBO17 and EBO24 in different lipid environments (supported lipid bilayer or MLV) and at different lipid/peptide ratios (Ri) obtained by fit of the ATR-IR spectra in the amide I region. Lipid composition: DMPC:DMPG:cholesterol:DMPE (6:2:5:3).

	EBO17			EBO24		
	Secondary structure	Wavenumber (cm^{-1})	% (±2.5)	Secondary structure	Wavenumber (cm^{-1})	% (±2.5)
In supported bilayer Ri = 150	β-sheet	1625–1632–1684	28.1	β-sheet	1622–1633–1683	24.4
	Random	1644	20.0	Random	1641	22.2
	α-helix	1652–1661	37.7	a-helix	1653	43.0
	β-turn	1673	14.2	β-turn	1670	13.4
In MLV Ri = 100	β-sheet	1625–1685	31.4	β-sheet	1625–1631–1685	38.8
	Random	1641	23.5	Random	1642	24.8
	α-helix	1655–1661	34.5	α-helix	1654–1662	28.8
	β-turn	1675	10.8	β-turn	1673	7.6
In MLV Ri = 20	β-sheet	1624–1683	39.1	β-sheet	1626–1683	50.0
	Random	1640	21.6	Random	1640	26.0
	α-helix	1655	30.5	α-helix	1651	11.0
	β-turn	1673	8.8	β-turn	1670	13.0

Table 2
Wavenumbers and dichroïc ratio of ν_{as} (CH_2) and ν_s (CH_2) of lipid chains and dichroïc ratio of ν(C═O) ester band around 1735 cm^{-1} in the absence and in the presence of EBO peptides. Lipid composition: DMPC:DMPG:cholesterol:DMPE (6:2:5:3).

		$\nu_{as}(CH_2)$ (cm^{-1})	$\nu_s(CH_2)$ (cm^{-1})	R_{ATR} ($\nu_s(CH_2)$)	R_{ATR} (ν(C═O))
Supported lipid bilayer	Alone	2920.7 ± 0,4	2851.7 ± 0,3	1.34 ± 0,05	1.67 ± 0,05
	+EBO17 −Ri = 150	2918.9 ± 0,4	2850.4 ± 0,3	1.24 ± 0,05	1.95 ± 0,05
	+EBO24 −Ri = 150	2919.4 ± 0,4	2850.8 ± 0,3	1.17 ± 0,05	2.07 ± 0,05
MLV	Alone	2920.1 ± 0,4	2851.0 ± 0,3	–	–
	+EBO17 −Ri = 100	2919.7 ± 0,5	2850.3 ± 0,1	–	–
	+EBO24 −Ri = 100	2918.5 ± 0,6	2850.3 ± 0,3	–	–
	+EBO17 −Ri = 20	2921.8 ± 0,5	2852.9 ± 0,3	–	–
	+EBO24 −Ri = 20	2921.9 ± 0,6	2853.4 ± 0,3	–	–

lipid chains from approximately 45° compared to the vertical for the lipid alone to 35–40° in the presence of EBO peptides [19]. Conversely, the dichroïc ratio of the ν(C═O) ester band of the lipids increases from 1.67 for the lipid alone to around 2.00 in the presence of the EBO peptide which is a characteristic of an increase of disorder. Altogether, this experiment is showing that whatever the EBO peptide, its insertion as a mainly vertical α-helix into the lipid bilayer at Ri = 150 leads to an increase of the order of the acyl chains but disorganizes the glycerol region of the lipids.

3.3.2. EBO17 and EBO24 inserted into multilamellar vesicles (MLV) at Ri = 100 and Ri = 20 by ATR spectroscopy

A single lipid bilayer could not be obtained using SUV bursting on the Ge crystal surface with the largest peptide content (Ri = 20) most likely because of the resulting SUV destabilization by the peptide. Consequently, EBO peptides have been incorporated in MLV using the same lipid mixture and ATR spectra have been recorded in solution (Fig. 6C and D), which allowed to estimate the peptide secondary structure content by fitting the amide I band (Table 1).

To compare with the results obtained with a single lipid bilayer at Ri = 150, MLV were first used at a lipid to peptide ratio of 100. The amide I region of spectra (Fig. 6C) was analyzed and the secondary structure content of the peptide bound to these MLV has then been evaluated from the analysis of the amide I band shape and curve fitting [15] (Table 1). It can be seen that the increase of the peptide content (Ri = 100) in MLV leads to an increase of the β-sheet content at the expense of the α-helical structure. The α-helix to β-sheet conversion is larger for the EBO24 peptide compared to the EBO17 peptide: +14.4% of β-sheets and −14.2% of α-helices for EBO24 compared to +3.3% of β-sheets and −3.2% of α-helices for EBO17. On EBO24, the β-sheet structure becomes predominant at Ri = 100 in MLV. Concerning lipid chain perturbation on MLV (Table 2), the same phenomenon is observed compared to the single bilayer at Ri = 150: there is an average decrease of −1.0 cm^{-1} and −0.7 cm^{-1} in the wavenumbers of the $\nu_{as}(CH_2)$ and $\nu_s(CH_2)$ respectively which suggests that the acyl chain order increased as a result of the EBO peptide insertion (Table 2).

At high peptide concentration (Ri = 20), a large increase of the β-sheet content can be observed both for EBO17 (39.1%) and for EBO24 (50.0%) compared to what has been obtained at Ri = 150 with the burst SUV or at Ri = 100 for the MLV (Fig. 6D, Table 1). Conversely, the α-helix content decreases while the random and β-turn contents remain comparable. We also investigated that the perturbation induced to the lipids upon EBO peptide binding has also been investigated by measuring the shift of $\nu_s(CH_2)$ and $\nu_{as}(CH_2)$ (Table 2). Whatever the EBO peptide at Ri = 20, a shift to higher wavenumber has been observed for $\nu_s(CH_2)$ and $\nu_{as}(CH_2)$ (+1.4 cm^{-1} for $\nu_{as}(CH_2)$, +1.9 to 2.4 cm^{-1} for $\nu_s(CH_2)$) in the presence of EBO peptides compared to the MLV alone which shows an increase of the chain disorder due to the EBO peptide insertion.

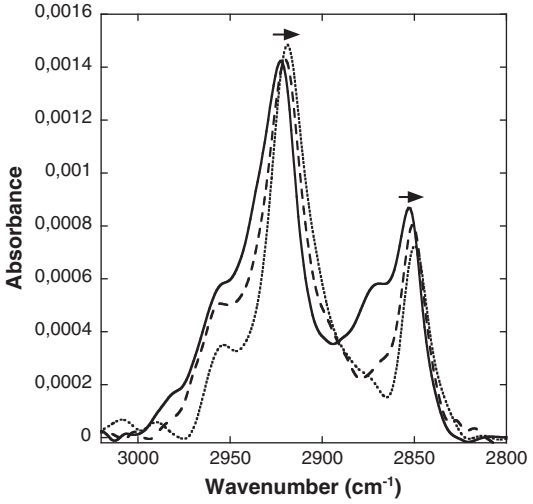

Fig. 7. ATR spectra in the 3000–2800 cm^{-1} region of a supported lipid bilayer DMPC:DMPG:cholesterol:DMPE (6:2:5:3) hydrated by D_2O + 150 mM NaCl: alone (solid line), +EBO17 Ri = 150 (dotted line), +EBO24 Ri = 150 (dotted line).

4. Discussion

4.1. Reversible conformational changes of EBO peptides

The IR results presented here show the structural polymorphism of the EBO peptides (EBO17 and EBO24) and their ability to change their conformation from an α-helix to antiparallel β-sheets. Such a transition occurs for the peptides alone at the air/water interface due to surface pressure increase as well as for the peptides inserted in lipid bilayers (single supported bilayer or MLV) due to the increase of the peptide concentration in the lipid system (Ri = 150 to Ri = 20). We can point out that as the surface pressure increases at the air/water interface, peptide surface density increases and so the concentration. Therefore, this α-to-β structural transition occurs with increasing peptide concentration. The comparable structural behavior of EBO17 and EBO24 shows that all the information required for this structural plasticity is contained in the 17 amino-acid sequence. As observed in our structural data (PMIRRAS and ATR), the lengthening of the sequence only allows to achieve structural folding at lower constraints (lower surface pressure and lower Ri). The ability of EBO17 to exist as an α-helix or as β-sheets was previously observed in a study where the authors showed a calcium dependent conformational change [7]. More generally, this ability to exist in these two structural states, or to modify their structure from an α-helix to antiparallel β-sheets seems to be a common behavior for several viral fusion peptides, as it was also observed for other class I fusion peptides such as FP23 fusion peptide of HIV-1 gp41 [19,36] and PIV5 fusion peptide of the Paramyxovirus [37] or the influenza hemagglutinin fusion peptide [38].

Such a common behavior can probably be explained by shared sequence characteristics like their enrichment in G and A residues (around 15% and 30% of amino-acid in their sequence respectively) at

relatively conserved positions conferring a structural plasticity [39]. But even if class I fusion peptides display some sequence similarities, the present data are showing that this conformational change can be reversible since a reverse transition was observed from antiparallel β-sheet to mainly α-helices upon surface pressure decrease of the monolayer. This reversible shift between α-helical and β-sheet structure was not observed for FP23 fusion peptide of HIV in the same time scale of experiments [19] but was observed for the first time with completely different peptide sequences involved in the intracellular membrane fusion of vesicles. Indeed, this α-helix to β-sheet conformational change was also observed in the transmembrane domain of SNARE proteins, $VAMP_{TM22}$ from VAMP1 and SYN_{TM23} from Syntaxin 1 depending on the lipid to peptide ratio [40]. These results illustrate some remarkable similarities on structural properties shared by totally different fusion processes such as class I viral fusion and intracellular fusion.

Actually, numerous studies demonstrate that a delicate balance between α and β structures, essential for protein-mediated viral membrane fusion is influenced by environmental conditions such as pH and ionic strength [41], the peptide sequence, presence or absence of divalent cations [7], the cholesterol content [36] and by the lipid/peptide ratio [36,42,43]. In the present study, we show that the conformational transition from an α-helix to a β-sheet is induced by a change in the peptide to lipid ratio in the membrane even in absence of calcium contrary to what Suarez and colleagues had previously suggested for EBO17 [7]. In our case, at low peptide concentration in lipids, EBO peptides (EBO17 and EBO24) interact with lipids mainly as α-helices. As the local peptide concentration increases in the membrane, the proportion of α-helix drops off in favor of a mainly antiparallel β-sheet structure. The formation of antiparallel β-sheet structure is probably due to the association of the peptides allowed by the close contacts induced by increasing concentration. This concentration dependent effect on peptide conformation might be of biological relevance. In the case of Ebola, experiments were made with a lipid to peptide ratio which potentially mimic the local concentrations of the peptide at the beginning of its insertion in the host membrane (Ri = 150 and Ri = 100) and its local gathering (Ri = 20) since several trimers of GP2 are thought to be involved in the fusion mechanism [44]. One can assume that during the fusion event, the Ebola fusion peptide inserts in the host membrane as an α-helix and then changes its conformation to a mainly β-sheet structure as its local concentration in the membrane increases, this structural plasticity being essential for the destabilization and lipid mixing taking place during membrane fusion processes [45,46]. Ebola GP shares general features with many other viral membrane fusion proteins. The more extensively studied HA1 and HA2 subunits from influenza virus are respectively analogous to the Ebola GP1 and GP2 subunits. Ebola glycoprotein GP2, like HA2, forms long trimeric coiled coils of α-helices (N-terminal α-helices) surrounded by a second layer of three shorter α-helices (C-terminal α-helices), creating a six helix-bundle in the late stage of fusion [47,48]. Although there is no direct evidence that the fusion peptide itself interacts with the C-terminal helices of GP2, its structural plasticity together with the reversibility of its structure could be of particular significance at this stage of the viral fusion.

4.2. Effect of EBO peptides on the lipid membrane organization

Our FTIR results suggest that, at low peptide content (Ri > 100), EBO peptides predominantly insert as α-helices oriented perpendicular to the plane of the lipid bilayer, which results in an increase of the order of the acyl chains of the lipids and a simultaneous destabilization of the lipid head groups. Although it is often difficult to properly compare experimental conditions and molecular modeling experiments in the determination of peptide orientation, the present result of a perpendicular orientation of the α-helical structure of the EBO peptides with respect to the plane of the membrane differs from that reported by Adam et al. [13]. Indeed, using molecular modeling, they found that the most stable orientation of a shorter EBO fusion peptide (first 11 residues of present EBO sequence) was 47° with respect the membrane plane. The effect of lipid chains increased order is in agreement with what was found by Gray and colleagues [38] who demonstrated that the lipid order parameter increases when the fusion peptide of hemagglutinin of influenza virus was incorporated into the bilayer at a lipid to peptide ratio of ~Ri = 150. One can speculate that this result may be related both to the high content of mainly vertically oriented α-helix which could organize the adjacent lipid chains by hydrophobic interactions and to the rearrangement of water molecules at the membrane interface in response to the binding of fusion peptides. Indeed, dehydration at the surface is known to increase the phase transition temperature in pure lipid bilayers [49] which is equivalent to an increase of the order of hydrocarbon chains in the hydrophobic core of lipid bilayers.

PMIRRAS and ATR data show that important perturbations of the lipid organization both in mono- and bilayer occur when the peptide concentration in the membrane was increased up to Ri = 20. PMIRRAS and Langmuir data showed that EBO peptide insertion leads to an important destabilization of the lipid monolayer, which results in to a loss of both lipids and peptides into the subphase during compression, presumably because of the disordering of the lipid monolayer by the EBO peptides. ATR data also showed that EBO peptide insertion at Ri = 20 leads to an important disorder in the lipid chain organization in the MLV bilayers. These results could allow to explain the impossibility to prepare SUV using mixtures of lipids and EBO peptides with at high peptide content. The ability of such fusion peptide to induce lipid chain disorder has previously been demonstrated for influenza fusion peptides where a change in membrane curvature was observed due to their ability to induce non bilayer lipid phases [50,51] for FP23 of HIV [19,52] as well as for FP of PIV5 where the β-sheet conformation promotes significant membrane curvature [37]. This common ability of fusion peptides to promote negative curvature, to lower the rupture tension of the lipid layers and to favor the formation of inverted phases is thought to be associated with initial steps of membrane fusion [53].

The present study shows the structural polymorphism of Ebola fusion peptide and demonstrates its ability to transit reversibly from a mainly α-helical structure to antiparallel β-sheets leading to a destabilization at large scale of the lipid membrane. As this structural flexibility is shared by different fusion processes (viral fusion, intracellular fusion), it could play a key role in the fusion mechanism. Therefore, it would be interesting to follow such type of fundamental study to get a complete understanding of interactions between fusion peptides and membranes.

Acknowledgements

We acknowledge Dr. Cyril Petibois and ANR-09-BLAN-0385-02 for their financial support.

References

[1] H. Feldmann, V.E. Volchkov, V.A. Volchkova, H.D. Klenk, The glycoproteins of Marburg and Ebola virus and their potential roles in pathogenesis, Arch. Virol. Suppl. 15 (1999) 159–169.
[2] S. Bar, A. Takada, Y. Kawaoka, M. Alizon, Detection of cell–cell fusion mediated by Ebola virus glycoproteins, J. Virol. 80 (2006) 2815–2822.
[3] A. Takada, C. Robison, H. Goto, A. Sanchez, K.G. Murti, M.A. Whitt, Y. Kawaoka, A system for functional analysis of Ebola virus glycoprotein, Proc. Natl. Acad. Sci. U. S. A. 94 (1997) 14764–14769.
[4] M. Brecher, K.L. Schornberg, S.E. Delos, M.L. Fusco, E.O. Saphire, J.M. White, Cathepsin cleavage potentiates the Ebola virus glycoprotein to undergo a subsequent fusion-relevant conformational change, J. Virol. 86 (2012) 364–372.
[5] W.R. Gallaher, Similar structural models of the transmembrane proteins of Ebola and avian sarcoma viruses, Cell 85 (1996) 477–478.
[6] M.S. Freitas, L.P. Gaspar, M. Lorenzoni, F.C. Almeida, L.W. Tinoco, M.S. Almeida, L.F. Maia, L. Degreve, A.P. Valente, J.L. Silva, Structure of the Ebola fusion peptide in a membrane-mimetic environment and the interaction with lipid rafts, J. Biol. Chem. 282 (2007) 27306–27314.
[7] T. Suarez, M.J. Gomara, F.M. Goni, I. Mingarro, A. Muga, E. Perez-Paya, J.L. Nieva, Calcium-dependent conformational changes of membrane-bound Ebola fusion peptide drive vesicle fusion, FEBS Lett. 535 (2003) 23–28.

[8] M.B. Ruiz-Arguello, F.M. Goni, F.B. Pereira, J.L. Nieva, Phosphatidylinositol-dependent membrane fusion induced by a putative fusogenic sequence of Ebola virus, J. Virol. 72 (1998) 1775–1781.
[9] M.J. Gomara, P. Mora, I. Mingarro, J.L. Nieva, Roles of a conserved proline in the internal fusion peptide of Ebola glycoprotein, FEBS Lett. 569 (2004) 261–266.
[10] M.S. Freitas, C. Follmer, L.T. Costa, C. Vilani, M.L. Bianconi, C.A. Achete, J.L. Silva, Measuring the strength of interaction between the Ebola fusion peptide and lipid rafts: implications for membrane fusion and virus infection, PLoS One 6 (2011) e15756.
[11] S. Sonnino, A. Prinetti, Membrane domains and the "lipid raft" concept, Curr. Med. Chem. 20 (2013) 4–21.
[12] A. Yonezawa, M. Cavrois, W.C. Greene, Studies of Ebola virus glycoprotein-mediated entry and fusion by using pseudotyped human immunodeficiency virus type 1 virions: involvement of cytoskeletal proteins and enhancement by tumor necrosis factor alpha, J. Virol. 79 (2005) 918–926.
[13] B. Adam, L. Lins, V. Stroobant, A. Thomas, R. Brasseur, Distribution of hydrophobic residues is crucial for the fusogenic properties of the Ebola virus GP2 fusion peptide, J. Virol. 78 (2004) 2131–2136.
[14] D. Blaudez, T. Buffeteau, J.C. Cornut, B. Desbat, N. Escafre, M. Pezolet, J.M. Turlet, Polarization modulation FTIR spectroscopy at the air–water interface, Thin Solid Films 242 (1994) 146–150.
[15] E. Goormaghtigh, V. Cabiaux, J.M. Ruysschaert, Secondary structure and dosage of soluble and membrane proteins by attenuated total reflection Fourier-transform infrared spectroscopy on hydrated films, Eur. J. Biochem. 193 (1990) 409–420.
[16] E. Goormaghtigh, V. Cabiaux, J.M. Ruysschaert, Determination of soluble and membrane protein structure by Fourier transform infrared spectroscopy. III. Secondary structures, Subcell. Biochem. 23 (1994) 405–450.
[17] E. Goormaghtigh, V. Raussens, J.M. Ruysschaert, Attenuated total reflection infrared spectroscopy of proteins and lipids in biological membranes, Biochim. Biophys. Acta 1422 (1999) 105–185.
[18] R.M.A. Azzam, N.M. Bashara, Ellipsometry and Polarized Light, North-Holland Publishing Co., Amsterdam, NY, 1977.
[19] S. Castano, B. Desbat, Structure and orientation study of fusion peptide FP23 of gp41 from HIV-1 alone or inserted into various lipid membrane models (mono-, bi- and multibi-layers) by FT-IR spectroscopies and Brewster angle microscopy, Biochim. Biophys. Acta 1715 (2005) 81–95.
[20] Z. Fezoua-Boubegtiten, B. Desbat, A. Brisson, S. Lecomte, Determination of molecular groups involved in the interaction of annexin A5 with lipid membrane models at the air–water interface, Biochim. Biophys. Acta 1798 (2010) 1204–1211.
[21] S. Castano, D. Blaudez, B. Desbat, J. Dufourcq, H. Wroblewski, Secondary structure of spiralin in solution, at the air/water interface, and in interaction with lipid monolayers, Biochim. Biophys. Acta 1562 (2002) 45–56.
[22] D. Blaudez, F. Boucher, T. Buffeteau, B. Desbat, M. Grandbois, C. Salesse, Anisotropic optical constants of bacteriorhodopsin in the mid-infrared: consequence on the determination of alpha-helix orientation, Appl. Spectrosc. 53 (1999) 1299–1304.
[23] D. Ducharme, J.J. Max, C. Salesse, R.M. Leblanc, Ellipsometric study of the physical states of phosphatidylcholines at the air–water interface, J. Phys. Chem. 94 (1990) 1925–1932.
[24] J. Saccani, S. Castano, B. Desbat, D. Blaudez, A phospholipid bilayer supported under a polymerized Langmuir film, Biophys. J. 85 (2003) 3781–3787.
[25] W.K. Surewicz, H.H. Mantsch, D. Chapman, Determination of protein secondary structure by Fourier transform infrared spectroscopy: a critical assessment, Biochemistry 32 (1993) 389–394.
[26] P.I. Haris, D. Chapman, Does Fourier-transform infrared spectroscopy provide useful information on protein structures? Trends Biochem. Sci. 17 (1992) 328–333.
[27] S. Castano, B. Desbat, M. Laguerre, J. Dufourcq, Structure, orientation and affinity for interfaces and lipids of ideally amphipathic lytic LiKj(i = 2j) peptides, Biochim. Biophys. Acta 1416 (1999) 176–194.
[28] S. Castano, B. Desbat, J. Dufourcq, Ideally amphipathic beta-sheeted peptides at interfaces: structure, orientation, affinities for lipids and hemolytic activity of (KL)(m)K peptides, Biochim. Biophys. Acta 1463 (2000) 65–80.
[29] A.-F. Mingotaud, C. Mingotaud, L.K. Patterson, Hanbook of Monolayers, Academic Press, San Diego, USA, 1993.
[30] J. Minones Jr., S. Pais, J. Minones, O. Conde, P. Dynarowicz-Latka, Interactions between membrane sterols and phospholipids in model mammalian and fungi cellular membranes — a Langmuir monolayer study, Biophys. Chem. 140 (2009) 69–77.
[31] H.H. Mantsch, R.N. McElhaney, Phospholipid phase transitions in model and biological membranes as studied by infrared spectroscopy, Chem. Phys. Lipids 57 (1991) 213–226.
[32] J.W. Brauner, R. Mendelsohn, F.G. Prendergast, Attenuated total reflectance Fourier transform infrared studies of the interaction of melittin, two fragments of melittin, and delta-hemolysin with phosphatidylcholines, Biochemistry 26 (1987) 8151–8158.
[33] M.W. Rooney, Y. Lange, J.W. Kauffman, Acyl chain organization and protein secondary structure in cholesterol-modified erythrocyte membranes, J. Biol. Chem. 259 (1984) 8281–8285.
[34] D.G. Cameron, H.L. Casal, H.H. Mantsch, Characterization of the pretransition in 1,2-dipalmitoyl-sn-glycero-3-phosphocholine by Fourier transform infrared spectroscopy, Biochemistry 19 (1980) 3665–3672.
[35] I.M. Asher, I.W. Levin, Effects of temperature and molecular interactions on the vibrational infrared spectra of phospholipid vesicles, Biochim. Biophys. Acta 468 (1977) 63–72.
[36] A.L. Lai, A.E. Moorthy, Y. Li, L.K. Tamm, Fusion activity of HIV gp41 fusion domain is related to its secondary structure and depth of membrane insertion in a cholesterol-dependent fashion, J. Mol. Biol. 418 (2012) 3–15.
[37] H. Yao, M. Hong, Membrane-dependent conformation, dynamics, and lipid interactions of the fusion peptide of the paramyxovirus PIV5 from solid-state NMR, J. Mol. Biol. 425 (2013) 563–576.
[38] C. Gray, S.A. Tatulian, S.A. Wharton, L.K. Tamm, Effect of the N-terminal glycine on the secondary structure, orientation, and interaction of the influenza hemagglutinin fusion peptide with lipid bilayers, Biophys. J. 70 (1996) 2275–2286.
[39] E.C. Smith, S.M. Gregory, L.K. Tamm, T.P. Creamer, R.E. Dutch, Role of sequence and structure of the Hendra fusion protein fusion peptide in membrane fusion, J. Biol. Chem. 287 (2012) 30035–30048.
[40] W. Yassine, N. Taib, S. Federman, A. Milochau, S. Castano, W. Sbi, C. Manigand, M. Laguerre, B. Desbat, R. Oda, J. Lang, Reversible transition between alpha-helix and beta-sheet conformation of a transmembrane domain, Biochim. Biophys. Acta 1788 (2009) 1722–1730.
[41] X. Han, L.K. Tamm, pH-dependent self-association of influenza hemagglutinin fusion peptides in lipid bilayers, J. Mol. Biol. 304 (2000) 953–965.
[42] J. Yang, D.P. Weliky, Solid-state nuclear magnetic resonance evidence for parallel and antiparallel strand arrangements in the membrane-associated HIV-1 fusion peptide, Biochemistry 42 (2003) 11879–11890.
[43] Y. Li, L.K. Tamm, Structure and plasticity of the human immunodeficiency virus gp41 fusion domain in lipid micelles and bilayers, Biophys. J. 93 (2007) 876–885.
[44] T.S. Jardetzky, R.A. Lamb, Virology: a class act, Nature 427 (2004) 307–308.
[45] P.K. Kinnunen, J.M. Holopainen, Mechanisms of initiation of membrane fusion: role of lipids, Biosci. Rep. 20 (2000) 465–482.
[46] D.J. Schibli, W. Weissenhorn, Class I and class II viral fusion protein structures reveal similar principles in membrane fusion, Mol. Membr. Biol. 21 (2004) 361–371.
[47] V.N. Malashkevich, B.J. Schneider, M.L. McNally, M.A. Milhollen, J.X. Pang, P.S. Kim, Core structure of the envelope glycoprotein GP2 from Ebola virus at 1.9-A resolution, Proc. Natl. Acad. Sci. U. S. A. 96 (1999) 2662–2667.
[48] W. Weissenhorn, L.J. Calder, S.A. Wharton, J.J. Skehel, D.C. Wiley, The central structural feature of the membrane fusion protein subunit from the Ebola virus glycoprotein is a long triple-stranded coiled coil, Proc. Natl. Acad. Sci. U. S. A. 95 (1998) 6032–6036.
[49] T.J. McIntosh, A.D. Magid, Phospholipid Hydration, in: G. Cevc (Ed.), Marcel Dekker, New york, USA, 1993.
[50] R.M. Epand, R.F. Epand, Relationship between the infectivity of influenza virus and the ability of its fusion peptide to perturb bilayers, Biochem. Biophys. Res. Commun. 202 (1994) 1420–1425.
[51] A. Colotto, R.M. Epand, Structural study of the relationship between the rate of membrane fusion and the ability of the fusion peptide of influenza virus to perturb bilayers, Biochemistry 36 (1997) 7644–7651.
[52] S. Promsri, G.M. Ullmann, S. Hannongbua, Molecular dynamics simulation of HIV-1 fusion domain–membrane complexes: insight into the N-terminal gp41 fusion mechanism, Biophys. Chem. 170 (2012) 9–16.
[53] B.G. Tenchov, R.C. MacDonald, B.R. Lentz, Fusion peptides promote formation of bilayer cubic phases in lipid dispersions, an X-ray diffraction study, Biophys. J. 104 (2013) 1029–1037.